energies

MDPI

Article

Thermophysical Properties of 1,1,1,3,3,3-Hexafluoro-2-methoxypropane (HFE-356mmz) in the Vapor Phase Measured by Using an Acoustic-Microwave Resonance Technique

Yuya Kano

National Institute of Advanced Industrial Science and Technology (AIST), Tsukuba 305-853, Japan; yuya-kano@aist.go.jp; Tel.: +81-29-861-4081

Received: 18 September 2020; Accepted: 19 October 2020; Published: 21 October 2020

Abstract: Thermophysical properties of HFE-356mmz in the vapor phase were measured by means of an acoustic-microwave resonance method. HFE-356mmz, which is 1,1,1,3,3,3-hexafluoro-2-methoxypropane in chemical name, is expected to be used as a working fluid with low global warming potential for the Organic Rankine cycle (ORC). The sound velocity and dielectric permittivity were simultaneously measured by using a cylindrical acoustic-microwave resonator. The sound velocity data were analyzed to obtain the ideal-gas heat capacity at constant pressure. The integral of the ideal-gas heat capacity as a function of temperature derives the ideal-gas enthalpy, which is a fundamental and important energy property to simulate the thermodynamic cycle. Similarly, the analysis of the dielectric permittivity data leads to information on the ideal-gas molar polarizability, dipole moment, and density. The acquired thermophysical properties of HFE-356mmz were compared to those of R-245fa and n-pentane, which are the existing working fluids for the ORC system, to prospect a feasibility of HFE-356mmz as their alternative.

Keywords: 1,1,1,3,3,3-hexafluoro-2-methoxypropane (HFE-356mmz); sound velocity; dielectric permittivity; heat capacity; molar polarization; dipole moment; density

1. Introduction

The Organic Rankin cycle (ORC) is one of the important thermal energy systems to efficiently utilize a waste heat below 100° C. Conventionally, 1,1,1,3,3-pentafluoropropane, which is known as R-245fa, has been used as a working fluid for the ORC. However, the global warming potential (GWP) of R-245fa is so high (858 [1]) that its production and use are internationally restricted under the Kigali Amendment to Montreal Protocol [2]. Although n-pentane is available as a natural hydrocarbon with a negligible GWP, and has also been used in the ORC, its high flammability is often concerned in terms of safety. Recently, 1,1,1,3,3,3-hexafluoro-2-methoxypropane, which is known as HFE-356mmz, has been proposed as an alternative working fluid for the ORC system [3]. HFE-356mmz has a flammability limit around 8.46 vol% [4] that is regarded as mildly flammable; however, it has a low GWP of 14 [1] and is not toxic. Thermophysical properties of a working fluid to be used in the ORC represent an indispensable information for the evaluation of the performance of the thermodynamic cycle. Some researchers previously reported experimental data of some thermophysical properties of HFE-356mmz; for example, Sako et al. [5] measured the critical properties and the normal boiling point, Alam et al. [6] measured the thermal conductivity and the kinematic viscosity, and Chen et al. [7] measured the pressure-volume-temperature (PVT) relation in the vapor phase.

In this study, the author simultaneously measured the sound velocity and the dielectric permittivity of HFE-356mmz in the vapor phase by means of an acoustic-microwave resonance method. The sound

velocity is related to heat capacity ratio of fluid since a sound wave at audio frequency adiabatically propagates in the fluid. Therefore, one can determine the ideal-gas heat capacities by extrapolating the measured sound velocity data to the limit of zero-density using the acoustic-virial equation. The ideal-gas heat capacities are an extremely important property to develop the thermodynamic equation of state of a working fluid, this being necessary to simulate and design a practical system for the realization of the thermodynamic cycle. On the other hand, the dielectric permittivity is associated with molecular polarization by the Clausius–Mossotti equation. In analogy with the sound velocity, the ideal-gas molar polarization, which means the molar polarization in the limit of zero-density, can be obtained from the intercept of the dielectric-virial equation fitted to the measured dielectric permittivity data. For a polar molecule with a permanent dipole moment, the ideal-gas molar polarization can be expressed as the Debye equation so that the dipole moment can be evaluated by analyzing its temperature dependence. Furthermore, information about density can be derived from the dielectric permittivity in combination with the dielectric-virial coefficients, which can be themselves determined by a polynomial regression of the dielectric-virial equation using the density-virial coefficients calculated on the basis of the corresponding state principle [8].

2. Experimental Setup

Concerning the sound velocity and dielectric permittivity measurements in the vapor phase, the experimental apparatus and fundamental equations used in this study are described in detail elsewhere [9,10]. Figure 1 illustrates a 3D overview of the cylindrical acoustic-microwave resonator used to measure the sound velocity and dielectric permittivity in this work. The length and diameter of the cylindrical cavity made of oxygen-free-copper are approximately 50 mm and 48 mm, respectively. The resonator is equipped with two microphones for measurement of acoustic resonances as well as two antennae for measurement of microwave resonances. An acoustic resonance frequency in the cylindrical cavity filled with a sample gas is measured by using an audio-frequency response analyzer to obtain the sound velocity. A value of the sound velocity at each temperature and pressure was determined from the measurement results for the acoustic resonance frequencies of four longitudinal modes, which were from (2, 0) mode to (5, 0) mode observed in a frequency range between 2 kHz and 7 kHz. Regarding the single longitudinal mode of (l, 0), the sound velocity, $w^{(l,0)}$, is expressed as the following relation.

$$w^{(l,0)} = \frac{2L_0(1+\chi p)}{l}\left(f_{r\_AC}^{(l,0)} + \Delta f_{r\_AC}^{(l,0)}\right) \tag{1}$$

In the above equation, L_0, χ, p, $f_{r\_AC}^{(l,0)}$, and $\Delta f_{r\_AC}^{(l,0)}$ represent the cylindrical cavity length under vacuum, the elastic compliance of the resonator, the sample gas pressure, the acoustic resonance frequency, and the frequency correction associated with the viscous and thermal boundary layers [9], respectively.

Similarly, a microwave resonance frequency in the cylindrical cavity is measured with a microwave vector network analyzer to obtain the dielectric permittivity. A value of the dielectric permittivity at each temperature and pressure was determined from the measurement results for the microwave resonance frequencies of four transverse magnetic (TM) modes, which were from TM010 mode to TM013 mode observed in a frequency range between 9 GHz and 14 GHz. For the single TM01s mode, the dielectric permittivity, $\varepsilon^{\mathrm{TM01s}}$, is expressed as the following relation.

$$\varepsilon^{\mathrm{TM01s}} = \left[\frac{\left(f_{r\_EM}^{vac\_\mathrm{TM01s}} + \Delta f_{r\_EM}^{vac\_TM01s}\right)}{\left(1+\frac{\chi p}{1+\chi p}\right)\left(f_{r\_EM}^{gas\_\mathrm{TM01s}} + \Delta f_{r\_EM}^{gas\_\mathrm{TM01s}}\right)}\right]^2 \tag{2}$$

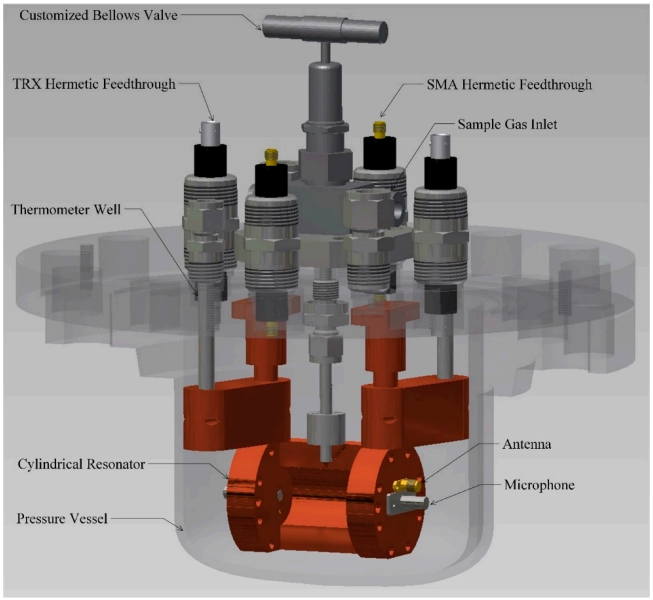

Figure 1. 3D overview of the cylindrical acoustic-microwave resonator.

In the above equation, $f_{r\_EM}^{gas\_\mathrm{TM01s}}$ and $f_{r\_EM}^{vac\_\mathrm{TM01s}}$ represent the microwave resonance frequencies in the gas filled and evacuated cavity, respectively, and $\Delta f_{r\_EM}^{gas\_\mathrm{TM01s}}$ and $\Delta f_{r\_EM}^{vac\_\mathrm{TM01s}}$ indicate their corrections associated with the skin-depth effect [9]. In addition, the microwave resonance frequencies in the evacuated cavity yield the cylindrical cavity dimensions at the measurement temperature, which is required to determine the sound velocity as shown in Equation (1).

The standard relative uncertainty for the sound velocity measurement is estimated to be typically 0.02%. Table 1 shows an example of the uncertainty budget for the sound velocity measurement at 343 K and 150 kPa. The measurement uncertainty of the sound velocity by the single mode mainly comes from that of the frequency correction, which are estimated from the excess half-width of the acoustic resonance. On the other hand, the standard relative uncertainty for the dielectric permittivity measurement is estimated to be from 0.02% to 0.19% depending on the sample gas temperature and pressure. Table 2 shows an example of the uncertainty budget for the dielectric permittivity measurement at 343 K and 150 kPa. The measurement uncertainty of the dielectric permittivity by the single mode also mainly arises from that of the frequency correction, which are estimated from the excess half-width of the microwave resonance. Both for the sound velocity and the dielectric permittivity, the standard uncertainties of the weighted means of the four mode results are statistically calculated from every single mode uncertainty in addition to the standard deviation of them.

Table 1. Uncertainty budget for the sound velocity measurement at 343 K and 150 kPa.

Factor of Uncertainty	(2, 0) Mode	(3, 0) Mode	(4, 0) Mode	(5, 0) Mode
Acoustic resonance frequency, $u\left(f_{r\_AC}^{(l,0)}\right)$	0.001%	0.001%	0.001%	0.001%
Frequency correction, $u\left(\Delta f_{r\_AC}^{(l,0)}\right)$	0.057%	0.020%	0.021%	0.026%
Cavity length, $u(L_0)$	0.011%	0.011%	0.011%	0.011%
Elastic compliance, $u(\chi)$	9×10^{-7}%	9×10^{-7}%	9×10^{-7}%	9×10^{-7}%
Sample gas pressure, $u(p)$	5×10^{-8}%	5×10^{-8}%	5×10^{-8}%	5×10^{-8}%
Covariance between $u(f_{r\_AC}^{(l,0)})$ & $u\left(\Delta f_{r\_AC}^{(l,0)}\right)$	0.011%	0.007%	0.007%	0.008%
Single mode result, $u\left(w^{(l,0)}\right)$	0.059%	0.024%	0.025%	0.030%
Standard deviation of the four modes	0.006%			
Weighted mean of the four modes, $u(w)$	0.016%			

Table 2. Uncertainty budget for the dielectric permittivity measurement at 343 K and 150 kPa.

Factor of Uncertainty	TM010 Mode	TM011 Mode	TM012 Mode	TM013 Mode
Microwave resonance frequency in gas, $u\left(f_{r\_EM}^{gas\_TM01s}\right)$	0.001%	0.001%	0.001%	0.003%
Microwave resonance frequency in vacuum, $u\left(f_{r\_EM}^{vac\_TM01s}\right)$	2×10^{-5}%	2×10^{-5}%	3×10^{-5}%	5×10^{-5}%
Frequency correction in gas, $u\left(\Delta f_{r\_EM}^{gas\_TM01s}\right)$	0.178%	0.188%	0.204%	0.215%
Frequency correction in vacuum, $u\left(\Delta f_{r\_EM}^{vac\_TM01s}\right)$	0.016%	0.034%	0.033%	0.046%
Elastic compliance, $u(\chi)$	2×10^{-6}%	2×10^{-6}%	2×10^{-6}%	2×10^{-6}%
Sample gas pressure, $u(p)$	1×10^{-7}%	1×10^{-7}%	1×10^{-7}%	1×10^{-7}%
Covariance between $u\left(f_{r\_EM}^{gas\_TM01s}\right)$ & $u\left(f_{r\_EM}^{vac\_TM01s}\right)$	-2×10^{-4}%	-2×10^{-4}%	-2×10^{-4}%	-6×10^{-4}%
Covariance between $u\left(f_{r\_EM}^{gas\_TM01s}\right)$ & $u\left(\Delta f_{r\_EM}^{gas\_TM01s}\right)$	0.014%	0.014%	0.020%	0.037%
Covariance between $u\left(f_{r\_EM}^{gas\_TM01s}\right)$ & $u\left(\Delta f_{r\_EM}^{vac\_TM01s}\right)$	−0.004%	−0.006%	−0.008%	−0.017%
Covariance between $u\left(f_{r\_EM}^{vac\_TM01s}\right)$ & $u\left(\Delta f_{r\_EM}^{gas\_TM01s}\right)$	−0.003%	−0.003%	−0.003%	−0.005%
Covariance between $u\left(f_{r\_EM}^{vac\_TM01s}\right)$ & $u\left(\Delta f_{r\_EM}^{vac\_TM01s}\right)$	0.001%	0.001%	0.001%	0.002%
Covariance between $u\left(\Delta f_{r\_EM}^{gas\_TM01s}\right)$ & $u\left(\Delta f_{r\_EM}^{vac\_TM01s}\right)$	−0.076%	−0.114%	−0.116%	−0.141%
Single mode result, $u\left(\varepsilon^{TM01s}\right)$	0.162%	0.155%	0.172%	0.172%
Standard deviation of the four modes	0.012%			
Weighted mean of the four modes, $u(\varepsilon)$	0.083%			

The cylindrical resonator is immersed in a liquid-bath temperature of which is precisely controlled within 5 mK. The temperature is measured using a standard platinum resistance thermometer, which is inserted in a thermometer well thermally contacted with the resonator, with a precision thermometer bridge. A pressure transducer using a quartz oscillation system, which is place at a headspace of the liquid-bath, directly measures the sample gas pressure. In order to compensate a pressure drift due to temperature, the zero-point of pressure under vacuum is measured at every measurement temperature and subtracted from the pressure readings. The standard uncertainties for the temperature and pressure measurements are estimated to be 10 mK and 0.2 kPa, respectively.

3. Measurement Results

3.1. Sound Velocity and Ideal-Gas Heat Capacity

The sample of HFE-356mmz was provided by Central Glass Co., Ltd., in Tokyo, Japan. The sample purity was analyzed by the supplier to be more than 99.9 mol%. Although the sample impurity component was not reported by the supplier, if it was assumed to be 0.1 mol% of the dry air, whose components were 78.12 mol% of Nitrogen, 20.96 mol% of Oxygen, and 0.92 mol% of Argon, the sound velocity would fractionally increase around 0.1% but the dielectric permittivity would not change beyond the measurement uncertainty. The gas sample was transferred into a stainless cylinder with 500 cm^3 volume, then it was purified by degassing as freezing a few times. Before the sample gas in the cylinder was introduced into the measurement system, it was flushed into the system several times to reduce an effect of the remaining gases in the experimental apparatus.

The sound velocity of HFE-356mmz was measured in a temperature range between 343 K and 423 K and in a pressure range of the vapor phase. Table 3 shows the sound velocity data for HFE-356mmz with their estimated standard uncertainties. Figure 2 also shows a pressure dependence of the sound velocity data on the five isotherms. The measured sound velocity data along each isotherm was analyzed using the following acoustic-virial equation [9].

$$w^2 = \frac{RTc_p^o}{M\left(c_p^o - R\right)}\left(1 + b_a p + c_a p^2\right) \tag{3}$$

Table 3. Sound velocity data in the vapor phase for HFE-356mmz.

T, K	*p*, kPa	*w*, m/s	*u*(*w*), m/s
343.15	50.6	126.10	0.02
343.15	70.6	125.10	0.02
343.15	89.3	124.17	0.02
343.15	119.3	122.68	0.02
343.15	152.4	120.99	0.02
363.06	50.3	130.09	0.03
363.06	80.5	128.80	0.03
363.06	120.4	127.11	0.03
363.06	162.0	125.24	0.03
363.05	199.1	123.56	0.03
383.02	51.0	133.75	0.02
383.02	104.4	131.89	0.02
383.02	160.7	129.88	0.02
383.03	220.7	127.69	0.02
383.03	287.4	125.15	0.02
403.03	99.6	136.08	0.02
403.03	199.2	133.10	0.02
403.03	299.3	130.01	0.02
403.04	399.6	126.74	0.02
403.04	497.0	123.37	0.02
423.05	121.6	139.51	0.02
423.05	201.1	137.42	0.02
423.05	302.6	134.81	0.02
423.06	500.8	129.40	0.02
423.05	703.1	123.37	0.02

In the above equation, w, M, c_p^o, R, T, and p indicate the sound velocity, the molar mass, the ideal-gas heat capacity at constant pressure, the gas constant, the temperature, and the pressure, respectively. Additionally, b_a and c_a are expressed as

$$b_a = \frac{B_a}{RT}, \tag{4}$$

$$c_a = \frac{C_a - B_\rho B_a}{(RT)^2}, \tag{5}$$

where B_a, C_a, and B_ρ represent the second acoustic-virial coefficient, the third acoustic-virial coefficient, and the second density-virial coefficient, respectively.

Fitting the sound velocity data on each isotherm to Equation (3), the ideal-gas heat capacity was obtained from the intercept value. Table 4 and Figure 3 show the ideal-gas heat capacity at constant pressure data for HFE-356mmz obtained through the above procedure. Error bars in Figure 3 indicate the estimated standard uncertainties corresponding to typically 4%. An estimated value of the ideal-gas heat capacity in accordance with the atomic-group contribution method by Joback and Reid [11] is also described in Figure 3. As seen in Figure 3, the present ideal-gas heat capacity shows a similar temperature dependence to the estimated one; however, its value is smaller than the estimated value by approximately 10%. Therefore, a new temperature correlation of the ideal-gas heat capacity for HFE-356mmz was formulated by using the Planck–Einstein equation.

$$c_p^o = 4R + \sum_{i=1}^{2} p_i \frac{(q_i/T)^2 \exp(q_i/T)}{(\exp(q_i/T) - 1)^2} \tag{6}$$

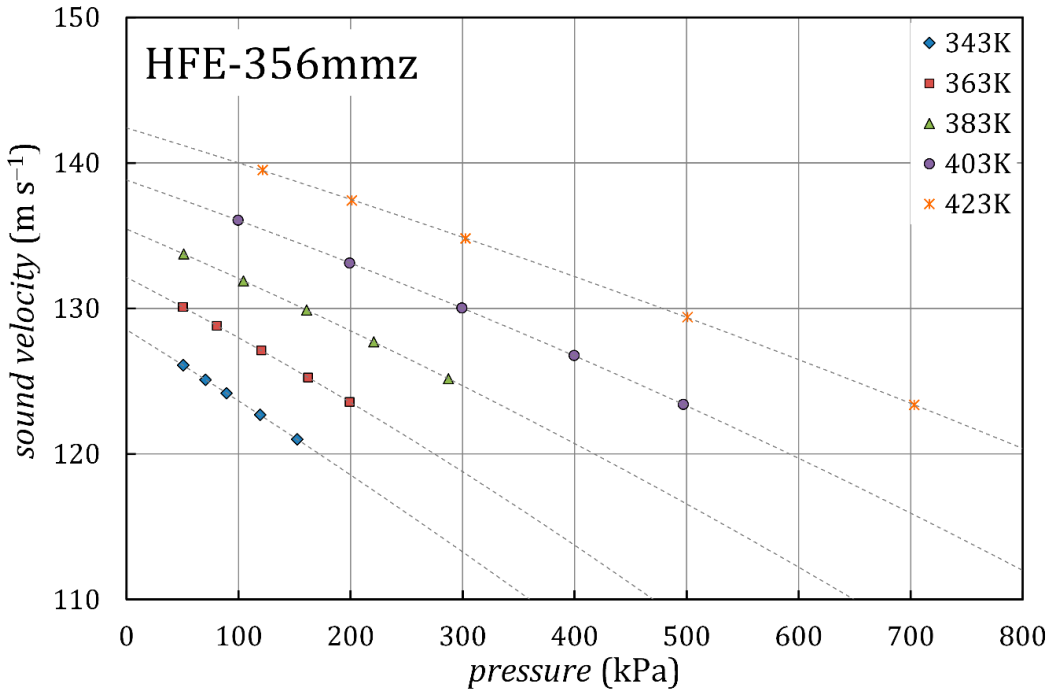

Figure 2. Sound velocity data on five isotherms for HFE-356mmz.

Table 4. Ideal-gas heat capacity at constant pressure data for HFE-356mmz.

T, K	c_p^o, J/(mol K)	$u(c_p^o)$ J/(mol K)
343.15	159.7	6.5
363.06	166.2	5.5
383.03	175.0	7.0
403.04	179.0	7.6
423.05	181.3	4.3

Numerical values of the coefficients in Equation (6) are listed in Table 5. The new correlation is also illustrated in Figure 3, reproducing the present ideal-gas heat capacity data with a standard deviation of about 0.9%. The ideal-gas Helmholtz free energy, which is a fundamental property to develop the thermodynamic equation of state for fluids, can be calculated from the integral of Equation (6) as a function of temperature [12].

Table 5. Numerical values of the coefficients in Equation (6).

Coefficient	Value
p_1	139.302
p_2	103.482
q_1	1474.761
q_2	424.514

3.2. Dielectric Permittivity and Ideal-Gas Molar Polarization

Measurement of the dielectric permittivity for HFE-356mmz was also carried out in the same temperature and pressure conditions as the sound velocity measurements. Table 6 summarizes the dielectric permittivity data of HFE-356mmz, meanwhile Figure 4 displays a pressure dependence of those along the five isotherms. It is obvious in Figure 4 that every measurement on the isotherms converges the dielectric permittivity of unity at the zero-pressure, which means the value is equal

to the permittivity of free space. In a similar way as the sound velocity, the dielectric permittivity data were fitted to the following dielectric-virial equation, which is expressed as an expansion of the Clausius–Mossotti equation regarding the dielectric permittivity [9].

$$\frac{\varepsilon-1}{\varepsilon+2}\frac{RT}{p} = A_\varepsilon^o + b_\varepsilon\left(\frac{\varepsilon-1}{\varepsilon+2}\right) + c_\varepsilon\left(\frac{\varepsilon-1}{\varepsilon+2}\right)^2 \tag{7}$$

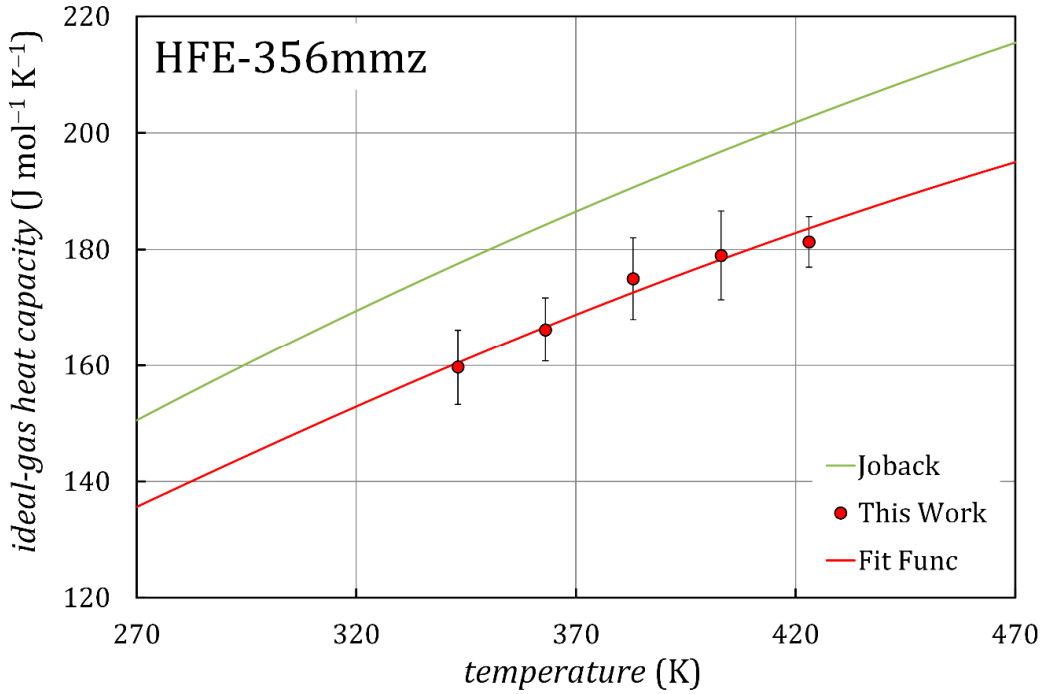

Figure 3. Temperature dependence of the ideal-gas heat capacity data for HFE-356mmz.

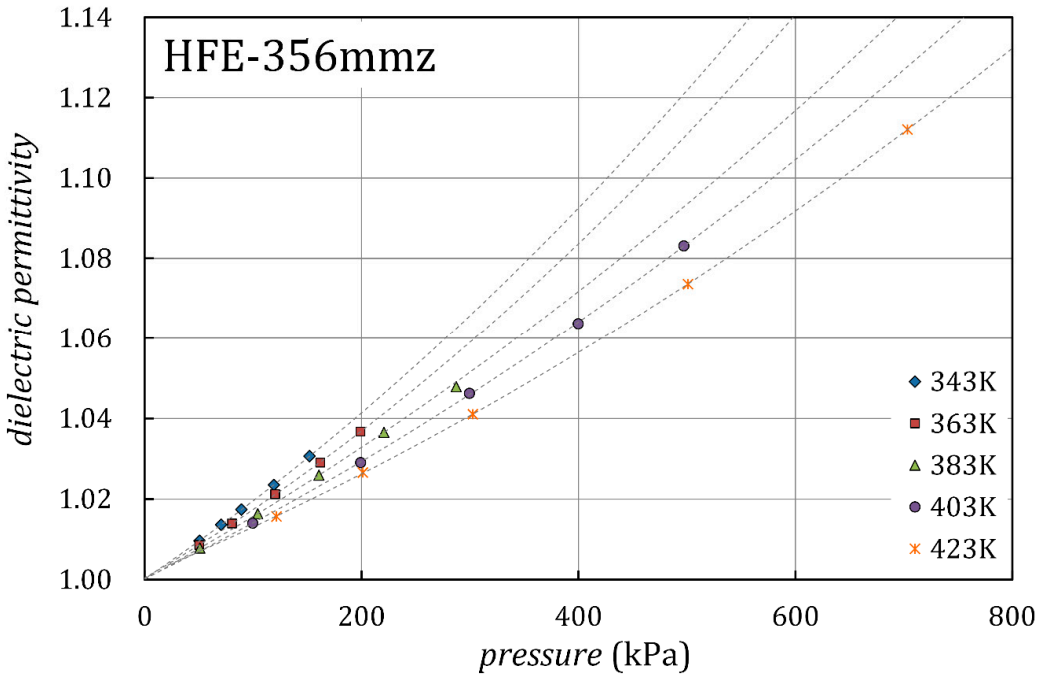

Figure 4. Dielectric permittivity data on five isotherms for HFE-356mmz.

Table 6. Dielectric permittivity data in the vapor phase for HFE-356mmz.

T, K	*p*, kPa	ε	$u(\varepsilon)$
343.15	50.6	1.00964	0.00021
343.15	70.6	1.01360	0.00031
343.15	89.3	1.01737	0.00046
343.15	119.3	1.02351	0.00064
343.15	152.1	1.03062	0.00086
363.06	50.4	1.00858	0.00018
363.06	80.6	1.01390	0.00032
363.06	120.4	1.02119	0.00054
363.06	162.0	1.02904	0.00079
363.05	199.0	1.03673	0.00102
383.03	51.1	1.00783	0.00016
383.02	104.4	1.01636	0.00042
383.03	160.7	1.02591	0.00073
383.02	220.7	1.03654	0.00104
383.03	287.3	1.04787	0.00132
403.04	99.7	1.01403	0.00034
403.03	199.3	1.02905	0.00080
403.03	299.4	1.04621	0.00121
403.03	399.7	1.06374	0.00152
403.04	497.1	1.08313	0.00190
423.05	121.7	1.01566	0.00039
423.04	201.2	1.02658	0.00069
423.04	302.7	1.04104	0.00121
423.05	501.0	1.07358	0.00160
423.05	703.2	1.11209	0.00211

In the above equation, ε and A_ε^o represent the dielectric permittivity and the ideal-gas molar polarization, respectively. In addition, b_ε and c_ε are given by

$$b_\varepsilon = \frac{B_\varepsilon - B_\rho A_\varepsilon^o}{A_\varepsilon^o}, \tag{8}$$

$$c_\varepsilon = \frac{A_\varepsilon^o C_\varepsilon - B_\varepsilon^2\left(B_\rho^2 - C_\rho\right)}{A_\varepsilon^{o3}}, \tag{9}$$

where B_ε, C_ε, and C_ρ indicate the second dielectric-virial coefficient, the third dielectric-virial coefficient, and the third density-virial coefficient, respectively.

The ideal-gas molar polarization of HFE-356mmz was determined from the intercept value of the polynomial regression for Equation (7) using the dielectric permittivity data on the isotherms. The results for the ideal-gas molar polarization of HFE-356mmz were summarized in Table 7. Figure 5 also illustrates the inverse temperature dependence of the ideal-gas molar polarization with its standard uncertainties, which correspond to typically 4%. As shown in Figure 5, the ideal-gas molar polarization is directly proportional to the inverse temperature in accordance with the Debye equation.

Table 7. Ideal-gas molar polarization data for HFE-356mmz.

T, K	A_ε^o, cm^3/mol	$u(A_\varepsilon^o)$, cm^3/mol
343.15	177.1	6.9
363.06	168.6	5.9
383.03	159.2	5.2
403.03	150.3	5.9
423.04	145.5	4.8

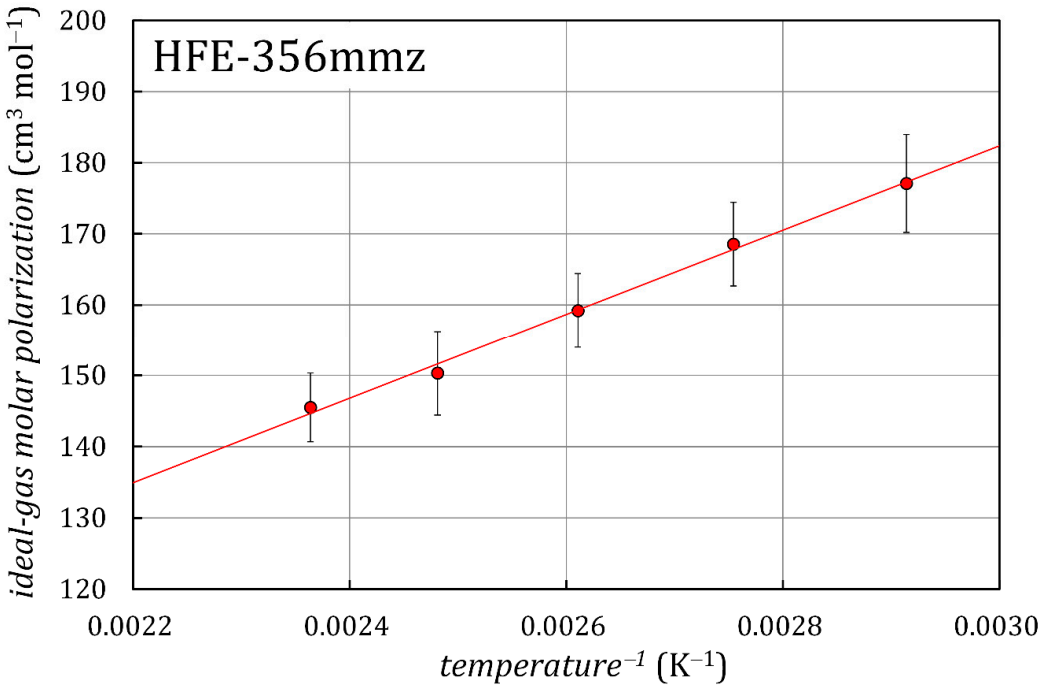

Figure 5. Inverse temperature dependence of the ideal-gas molar polarization data for HFE-356mmz.

3.3. Dipole Moment and Density

As stated in the previous section, the ideal-gas molar polarization is expressed as the Debye equation given by

$$A_\varepsilon^o = \alpha + \frac{\beta}{T}, \tag{10}$$

where α and β correspond to the polarization of the electronic and atomic displacement shown in Equation (11) and that of the dipole orientation shown in Equation (12), respectively.

$$\alpha = \frac{N_A \alpha_m}{3\varepsilon_0} \tag{11}$$

$$\beta = \frac{N_A \mu_m^2}{9\varepsilon_0 k_B} \tag{12}$$

In the above equations, N_A, α_m, ε_0, μ_m, and k_B represent the Avogadro constant, the molecular polarizability, the permittivity of free space, the permanent dipole moment, and the Boltzmann constant, respectively. Consequently, the dipole moment is derived from the value of β in Equation (12), which corresponds to the slope of the ideal-gas molar polarization dependence on inverse temperature. The linear regression analysis based on the results of the ideal-gas molar polarization in Figure 5 leads to an estimate for the dipole moment of 3.12 D for HFE-356mmz, where 1 D is equivalent to (10^{-21}/299,792,458) C m. The standard uncertainty of the dipole moment was estimated at 0.06 D or 1.9% in the relative uncertainty.

Moreover, the density of HFE-356mmz was extracted from the dielectric permittivity measurements in accordance with the thermodynamic relation given by [13],

$$\rho = a_\rho + b_\rho a_\rho^2 + c_\rho a_\rho^3, \tag{13}$$

where a_ρ, b_ρ, and c_ρ are expressed as the following equations.

$$a_\rho = \frac{(\varepsilon - 1)}{A_\varepsilon^o(\varepsilon + 2)} \tag{14}$$

$$b_\rho = \frac{-B_\varepsilon}{A_\varepsilon^o} \tag{15}$$

$$c_\rho = \frac{2B_\varepsilon^2 - A_\varepsilon^o C_\varepsilon}{A_\varepsilon^{o2}} \tag{16}$$

The dielectric-virial coefficients appearing in Equations (14)–(16) were determined such that the dielectric permittivity data were fitted to Equation (7) by using the deduced density-virial coefficients on the basis of the corresponding state principle as follows [8].

$$B_\rho\left(\frac{p_c}{RT_c}\right) = F_{B0}(T_r) + \omega F_{B1}(T_r) + F_{B2}(T_r) \tag{17}$$

$$C_\rho\left(\frac{p_c}{RT_c}\right)^2 = C_0 + \left\{B_\rho\left(\frac{p_c}{RT_c}\right) + C_1\right\}^2 \{F_{C0}(T_r) + F_{C1}(T_r)\} \tag{18}$$

In the above equations, p_c, T_c, T_r, and ω indicate the critical pressure, the critical temperature, the reduced temperature, and the acentric factor, respectively, and the function forms as well as the coefficients are described in the reference [8]. The critical parameters and the acentric factor for HFE-356mmz are available in the reference [5]. Since the final terms in the right-hand side of Equations (17) and (18) are the functions containing the dipole moment, the value determined in this work was employed to estimate the density virial coefficients. Table 8 shows the results for the density data of HFE-356mmz with the estimated standard uncertainties, which correspond to typically 4%. Figures 6 and 7 illustrate the pressure dependence of the density on the five isotherms and the pressure deviation of the present PVT data from the virial equation by Chen et al. [7], respectively. It was found from Figure 7 that the present data are consistent with the reference equation almost within 2%. According to the reference [7], the virial equation reproduces the PVT data with a maximum pressure deviation of 1.984%. Therefore, most of the present data agreed well within the uncertainty of the virial equation.

Table 8. Density data in the vapor phase for HFE-356mmz.

T, K	*p*, kPa	ρ, kg/m^3	$u(\rho)$, kg/m^3
343.15	50.6	3.31	0.15
343.15	70.6	4.67	0.21
343.15	89.3	5.96	0.28
343.15	119.3	8.06	0.38
343.15	152.1	10.47	0.50
363.06	50.4	3.10	0.13
363.06	80.6	5.02	0.21
363.06	120.4	7.62	0.33
363.06	162.0	10.38	0.45
363.05	199.0	13.00	0.55
383.03	51.1	2.97	0.11
383.02	104.4	6.15	0.25
383.03	160.7	9.66	0.41
383.02	220.7	13.50	0.57
383.03	287.3	17.51	0.72
403.04	99.7	5.56	0.25
403.03	199.3	11.32	0.52
403.03	299.4	17.70	0.80
403.03	399.7	24.05	1.06
403.04	497.1	30.95	1.37
423.05	121.7	6.46	0.26
423.04	201.2	10.88	0.45
423.04	302.7	16.60	0.71
423.05	501.0	28.88	1.07
423.05	703.2	42.22	1.44

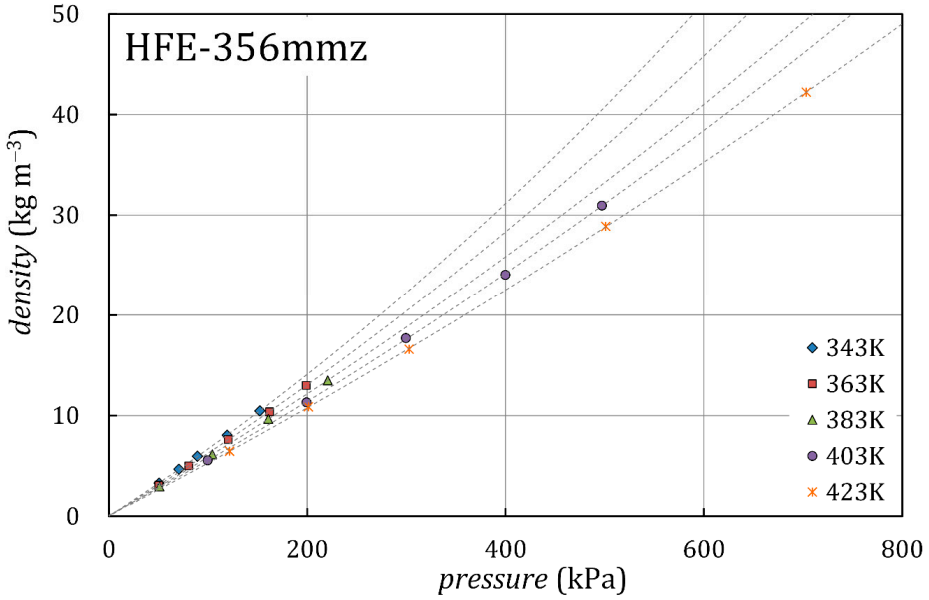

Figure 6. Density data on five isotherms for HFE-356mmz.

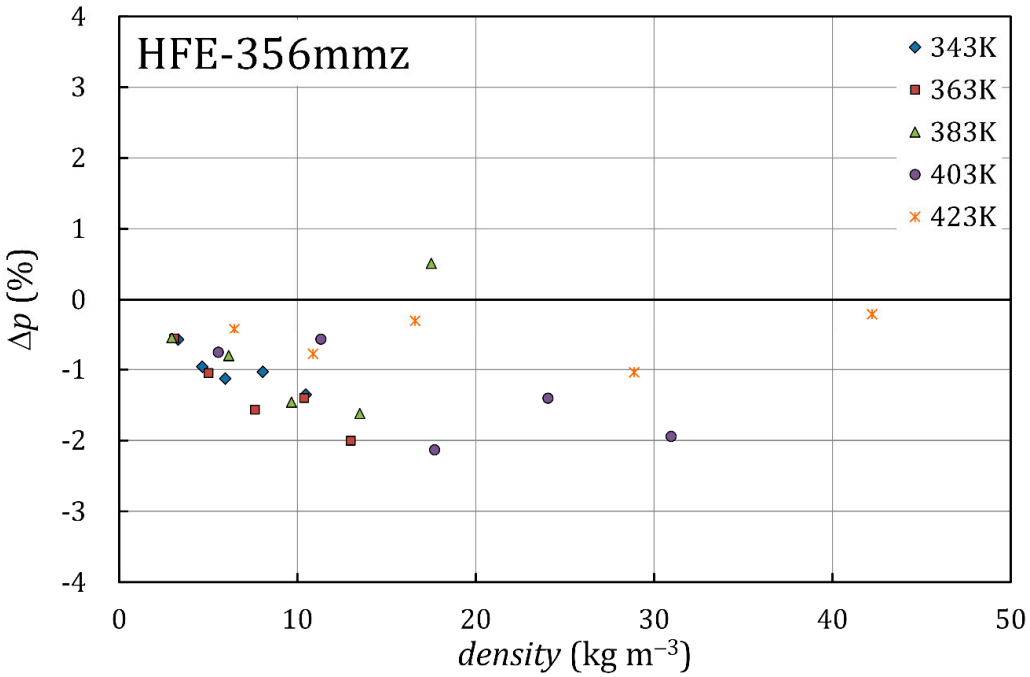

Figure 7. Pressure deviation of the present pressure-volume-temperature (PVT) data from the virial equation by Chen et al. [7] for HFE-356mmz. The base line corresponds to the pressure calculated from the virial equation.

4. Discussion

In this section, the determined thermophysical properties of HFE-356mmz are compared with those for R-245fa and n-pentane according to the reference database of REFPROP ver. 10, NIST, in Boulder, CO, USA [14]. Figures 8–10 display the relative differences of the sound velocity, dielectric permittivity, and density, respectively, under the same temperature and pressure conditions. Unfortunately, the dielectric permittivity of R-245fa cannot be calculated by REFPROP so its comparison is not included in Figure 9. For the sound velocity, HFE-356mmz is lower than R-245fa and n-pentane by approximately 20% and 60%, respectively. On the other hand, the density of HFE-356mmz is higher

than that of R-245fa by around 30% and that of n-pentane by around 60%. Regarding the dielectric permittivity, HFE-356mmz is higher than n-pentane by about 1% to 10% depending on the pressure.

Furthermore, Figure 11 shows a comparison of the ideal-gas heat capacity at constant pressure of HFE-356mmz with that of R-245fa and n-pentane. As shown in Figure 11, the ideal-gas heat capacity of HFE-356mmz is higher than that of R-245fa by approximately 20% and that of n-pentane by approximately 10–18% depending upon the temperature. Using the temperature correlation in Equation (6), the ideal-gas enthalpy, h^o, can be calculated from the following relation [15].

$$h^o = h_0 + 4R(T - T_0) + \sum_{i=1}^{2} p_i q_i \frac{\exp(q_i/T)}{\exp(q_i/T) - 1} - \sum_{i=1}^{2} p_i q_i \frac{\exp(q_i/T_0)}{\exp(q_i/T_0) - 1} \quad (19)$$

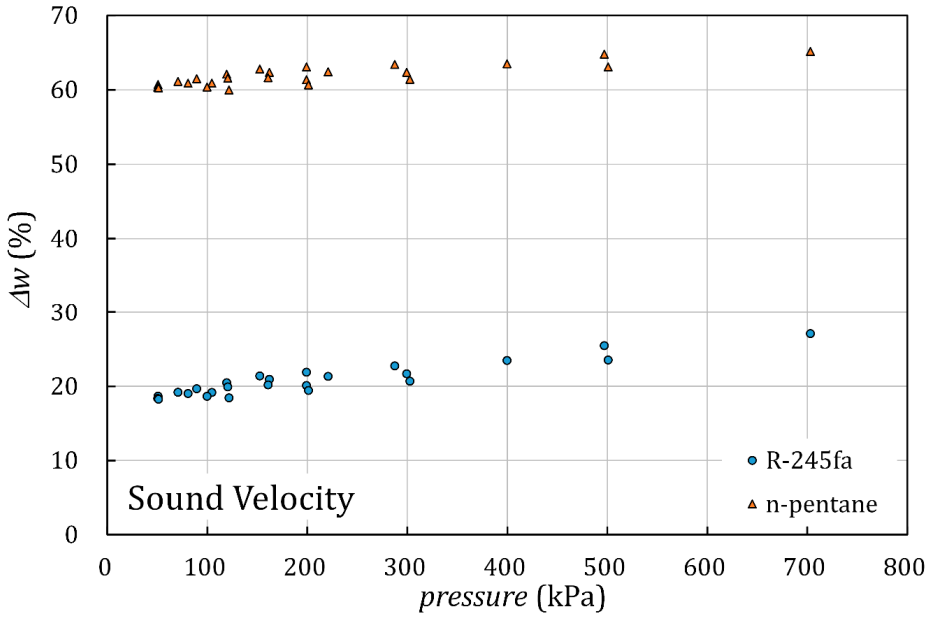

Figure 8. Comparison of the sound velocity of HFE-356mmz with that of R-245fa and n-pentane. The base line corresponds to the sound velocity of HFE-356mmz.

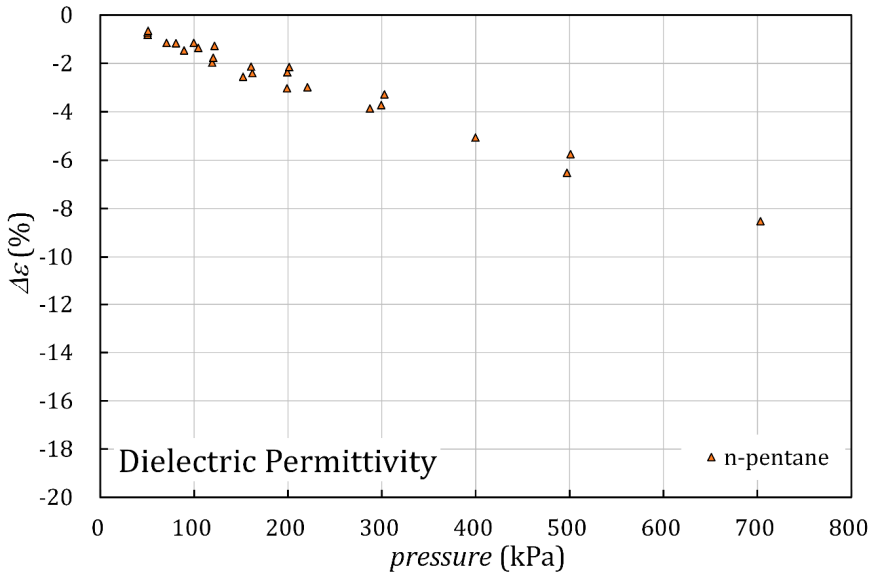

Figure 9. Comparison of the dielectric permittivity of HFE-356mmz with that of n-pentane. The base line corresponds to the dielectric permittivity of HFE-356mmz.

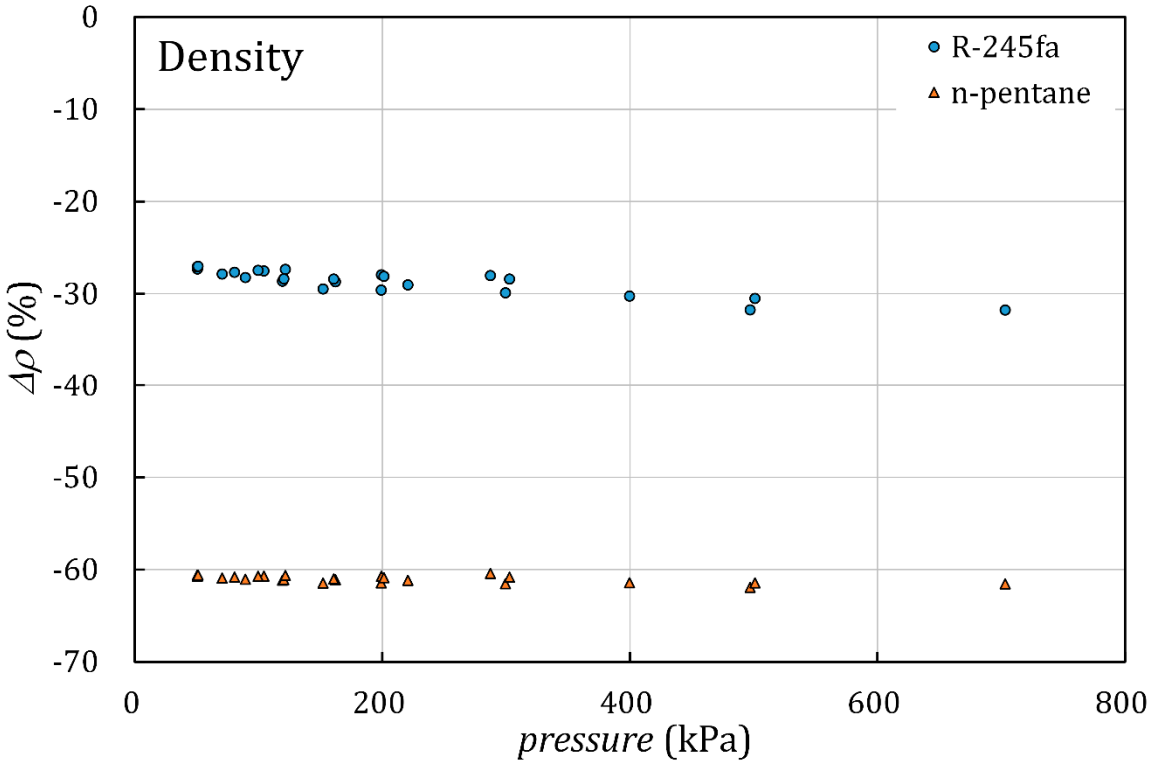

Figure 10. Comparison of the density of HFE-356mmz with that of R-245fa and n-pentane. The base line corresponds to the density of HFE-356mmz.

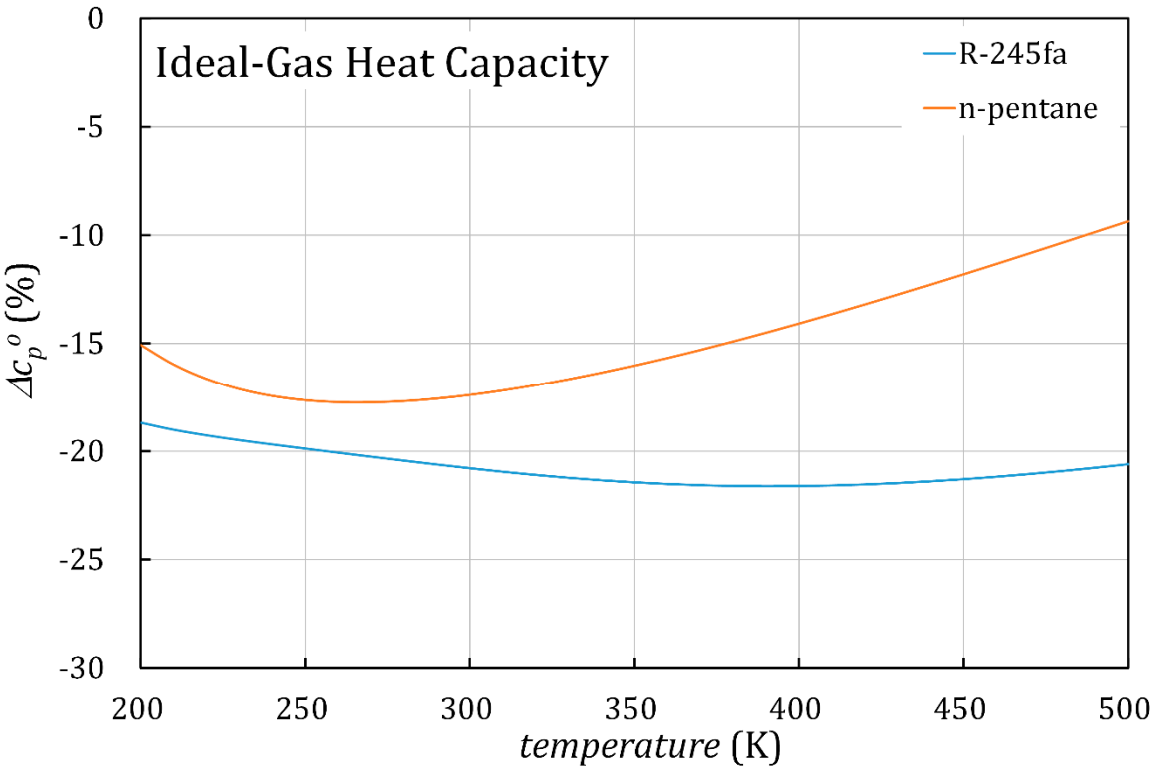

Figure 11. Comparison of the ideal-gas heat capacity at constant pressure of HFE-356mmz with that of R-245fa and n-pentane. The base line corresponds to the ideal-gas heat capacity of HFE-356mmz.

In the above equation, h_0 and T_0 are the values of the enthalpy and temperature at an arbitrary reference state, respectively. In this work, the reference state is set as the enthalpy equal to 0 kJ/kg at 273.15 K in the ideal gas state. Figure 12 shows the calculated ideal-gas enthalpy per mol of HFE-356mmz. Compared with the ideal-gas enthalpies per mol of R-245fa and n-pentane with the same reference state, that of HFE-356mmz has the largest value. At 373.15 K, the ideal-gas enthalpy per mol of HFE-356mmz is larger than that of R-245fa by about 3.2 kJ/mol and that of n-pentane by about 2.6 kJ/mol, and these differences increase at 473.15 K by about 7.2 kJ/mol and 4.9 kJ/mol, respectively. However, the molar mass of HFE-356mmz (M = 182.06 g/mol) is larger than those of R-245fa (M = 134.05 g/mol) and n-pentane (M = 72.15 g/mol) so that the ideal-gas enthalpy per mass of HFE-356mmz has the lowest value as shown in Figure 13. At 373.15 K, the ideal-gas enthalpy per mass of HFE-356mmz is lower than that of R-245fa by around 6.0 kJ/kg and that of n-pentane by around 93.1 kJ/kg, and these differences become larger at 473.15 K by 12.8 kJ/kg and 213.6 kJ/kg, respectively. The result of Figure 13 implies that a performance of the thermodynamic cycle using HFE-356mmz as a working fluid is possibly close to that using R-245fa under the same cycle condition, although the residual part of enthalpy for the real fluid, which is dependent upon not only temperature but also density, must be examined to evaluate the cycle performance accurately.

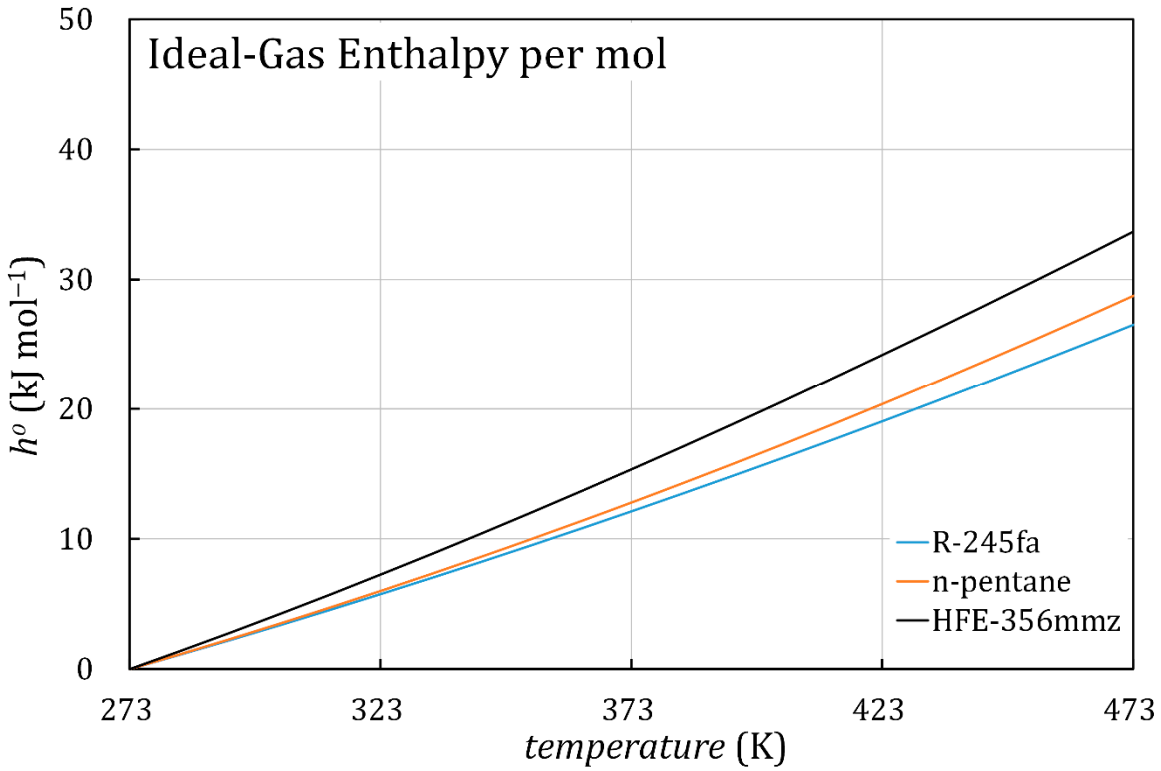

Figure 12. Comparison of the ideal-gas enthalpy per mol of HFE-356mmz with that of R-245fa and n-pentane.

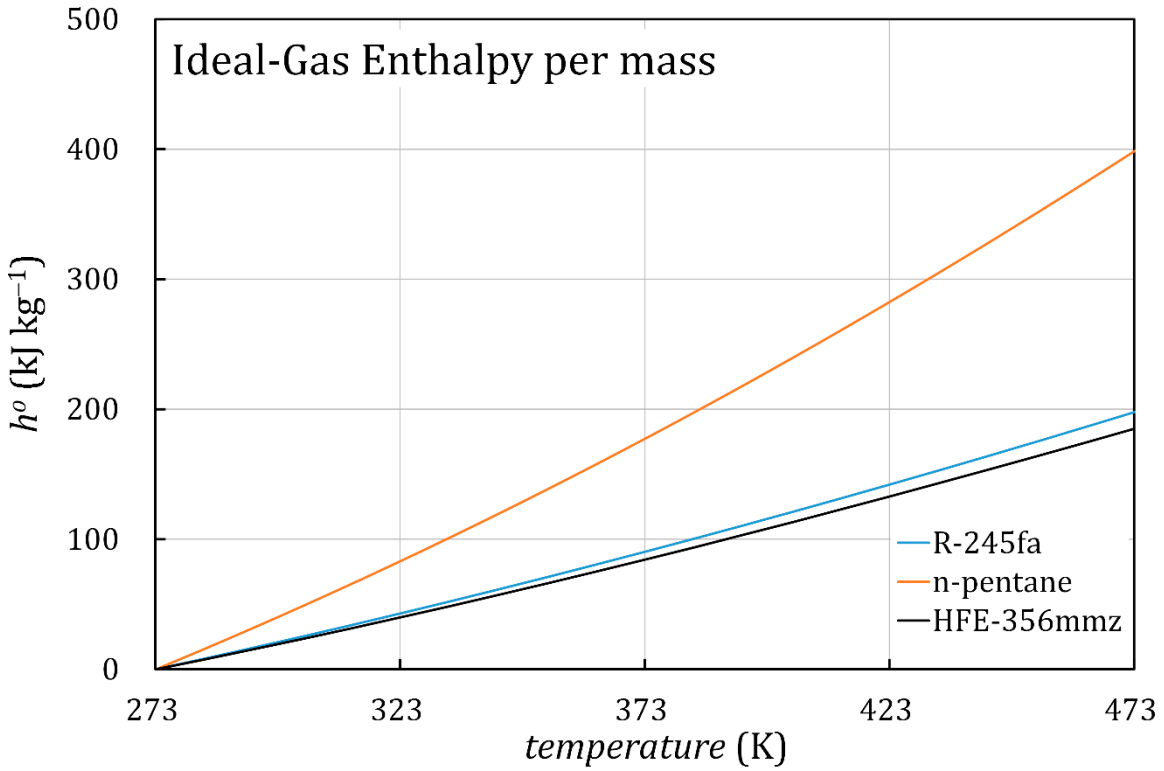

Figure 13. Comparison of the ideal-gas enthalpy per mass of HFE-356mmz with that of R-245fa and n-pentane.

Additionally, the values of the dipole moment are 1.55 D for R-245fa and 0.07 D for n-pentane [14]. Since the dipole moment of HFE-356mmz determined in this work is 3.12 D, the molecule of HFE-356mmz has stronger polarity than those of R-245fa and n-pentane. The polarity of a molecule is one of the characteristics to be associated with the solubility to the other molecule, so that the lubricant used with R-245fa or n-pentane in the existing ORC system is possibly not suitable for HFE-356mmz.

5. Conclusions

Several thermophysical properties of HFE-356mmz in the vapor phase were experimentally determined in this study. The sound velocity and the dielectric permittivity were simultaneously measured by using the acoustic-microwave resonance method. The analysis of the obtained sound velocity data yielded the ideal-gas heat capacity at constant pressure, meanwhile that of the obtained dielectric permittivity data derived the ideal-gas molar polarization, the dipole moment, and the density. Compared with the thermophysical properties of R-245fa and n-pentane, which are the existing working fluids for the ORC system, HFE-356mmz has a lower value for the sound velocity and a higher value for the density and the ideal-gas heat capacity under the same thermodynamic equilibrium state. A comparison of the dipole moment revealed that HFE-356mmz has stronger polarity than R-245fa and n-pentane. Moreover, the ideal-gas enthalpy was calculated from the temperature correlation of the ideal-gas heat capacity, and it was found that HFE-356mmz has possibility to be comparable to R-245fa in the ORC system. The acquired thermophysical properties data of HFE-356mmz in this work are valuable information not only to develop the thermodynamic equation of state but also to optimize the ORC system in practice.

Funding: This study was partially supported by JSPS KAKENHI Grant Number JP17H04908.

Acknowledgments: The author would express my gratitude to Thermal Management Materials and Technology Research Association (TherMAT), Japan for providing the information of HFE-356mmz, and to Central Glass Co. Ltd. for supplying the high purity sample of HFE-356mmz.

Conflicts of Interest: The author declares no conflict of interest.

References

1. Myhre, G.; Shindell, D.; Bréon, F.-M.; Collins, W.; Fuglestvedt, J.; Huang, J.; Koch, D.; Lamarque, J.-F.; Lee, D.; Mendoza, B.; et al. Anthropogenic and Natural Radiative Forcing. In *Climate Change 2013: The Physical Science Basis. Contribution of Working Group I to the Fifth Assessment Report of the Intergovernmental Panel on Climate Change*; Stocker, T.F., Qin, D., Plattner, G.-K., Tignor, M., Allen, S.K., Boschung, J., Nauels, A., Xia, Y., Bex, V., Midgley, P.M., Eds.; Cambridge University Press: Cambridge, UK; New York, NY, USA, 2013; pp. 659–740.
2. Heath, E.A. Amendment to the Montreal Protocol on Substances that Deplete the Ozone Layer (Kigali Amendment). *Int. Leg. Mater.* **2017**, *56*, 193–205. [CrossRef]
3. Sekiya, A.; Misaki, S. The potential of hydrofluoroethers to replace CFCs, HCFCs and PFCs. *J. Fluor. Chem.* **2000**, *101*, 215–221. [CrossRef]
4. Kondo, S.; Urano, Y.; Takizawa, K.; Takahashi, A.; Tokuhashi, K.; Sekiya, A. Flammability limits of multi-fluorinated compounds. *Fire Saf. J.* **2006**, *41*, 46–56. [CrossRef]
5. Sako, T.; Yasumoto, M.; Sato, M.; Kitao, O.; Ishiguro, K.; Kato, M. Measurement of critical properties of fluorinated ethers and amines. *Fluid Phase Equilib.* **1998**, *144*, 113–117. [CrossRef]
6. Alam, J.M.; Kariya, K.; Yamaguchi, K.; Hori, Y.; Miyara, A. Measurement of thermal conductivity and kinematic viscosity of 1,1,1,3,3,3-hexafluoro-2-methoxypropane (HFE-356mmz). *Int. J. Refrig.* **2019**, *103*, 1–8. [CrossRef]
7. Chen, Q.; Gao, R.; Guan, X.; Du, L.; Chen, G.; Tang, L. Measurement and correlation of gaseous pvt property for 1,1,1,3,3,3-hexafluoro-2-methoxypropane (HFE-356mmz). *J. Chem. Eng. Data* **2020**, *65*, 4230–4235. [CrossRef]
8. Meng, L.; Duan, Y.Y.; Li, L. Correlations for second and third virial coefficients of pure fluids. *Fluid Phase Equilib.* **2004**, *226*, 109–120. [CrossRef]
9. Kano, Y.; Kayukawa, Y.; Fujita, Y. Dipole moment and heat capacity in the ideal gas state derived from relative permittivity and speed of sound measurements for HFO-1123 and HCFO-1224yd(Z). *Int. J. Refrig.* **2020**, *118*, 354–364. [CrossRef]
10. Kano, Y. Multi-property evaluation for a gas sample based on the acoustic and electromagnetic resonances measurement in a cylindrical cavity. *J. Chem. Thermodyn.* **2020**. submitted for publication.
11. Joback, K.G.; Reid, R.C. Estimation of pure-component properties from group-contributions. *Chem. Eng. Commun.* **1987**, *57*, 233–243. [CrossRef]
12. Richter, M.; McLinden, M.O.; Lemmon, E.W. Thermodynamic properties of 2,3,3,3-tetrafluoroprop-1-ene (R1234yf): Vapor pressure and *p-r-T* measurements and an equation of state. *J. Chem. Eng. Data* **2011**, *56*, 3254–3264. [CrossRef]
13. St-Arnaud, J.M.; Hourri, A.; Okambawa, R.; Belanger, M. Determination of the density in the gas phase with a computer-controlled measuring system of the dielectric constant. *Rev. Sci. Instrum.* **1995**, *66*, 5311–5316. [CrossRef]
14. Lemmon, E.W.; Bell, I.H.; Huber, M.H.; McLinden, M.O. *REFPROP—NIST Standard Reference Database 23. Version 10.0*; National Institute of Standard and Technology: Boulder, CO, USA, 2018.
15. Lemmon, E.W.; Span, R. Short fundamental equations of state for 20 industrial fluids. *J. Chem. Eng. Data* **2006**, *51*, 785–850. [CrossRef]